THERMODYNAMIC AND HEAT TRANSFER EVALUATION OF A THERMIC SOLAR PANEL

by

A. KEN YASUDA

Submitted in Partial Fufillment
of the Requirements for the
Degree of Bachelor of Science

at the

MASSACHUSETTS INSTITUTE OF TECHNOLOGY

May, 1976

Signature redacted

Signature of Author.....
Department of Mechanical Engineering, May 17, 1976

Signature redacted

Certified by.....
Thesis Supervisor

Signature redacted

Accepted by.....
Chairman, Departmental Committee on Theses

THERMODYNAMIC AND HEAT TRANSFER EVALUATION OF A THERMIC SOLAR PANEL

by

A. KEN YASUDA

Submitted to the department of Mechanical Engineering on May 17, 1976 in partial fulfillment of the requirements for the Degree of Bachelor of Science.

ABSTRACT

The rising concern over coal, oil, and natural gas reserves has led to the examination of alternative energy resources such as solar energy for home heating. Massachusetts Institute of Technology has developed the concept of a thermic diode solar panel for space heating. Computer simulations of this panel have been made and a scale model tested. A full size solar panel has also been constructed. The purpose of this study is to evaluate the performance of this prototype under actual weather conditions. The efficiency of the solar collector and of the overall panel have been evaluated empirically under specified ambient conditions. Over one day, the solar collector will transfer 44% of the incident solar radiation into the storage section. Of this, 11% can be utilized for space heating.

Thesis Supervisor: B. Shawn Buckley

Title: Associate Professor of Mechanical Engineering
Massachusetts Institute of Technology

TABLE OF CONTENTS

LIST OF FIGURES

LIST OF TABLES

INTRODUCTION

The thermic panel is an independent unit which contains both the solar collector and heat storage section. The thermic panel is shown in Figure 1. The panel has three important elements: the sensor layer(solar collector), the storage layer, and the control box which modulates flow between sensor and storage. The panel operates like a thermal siphon. When solar radiation strikes the sensor layer, the water within the sensor layer is heated and expands. The storage layer remains cool, and has a higher density. This density difference results in a pressure head differential which then drives the water from the sensor layer through the control box and into the storage layer. After the storage layer has been sufficiently heated, a forced air system is used to draw the heat off. The heated air may then be circulated through the house. When there is no demand for heat, the forced air fan may be shut off and the heat saved in the storage layer.

The solar radiation decreases in the afternoon, so by late afternoon the storage layer temperature has risen sufficiently to nullify the driving head. As the sun sets there is a pressure head in the opposite direction.

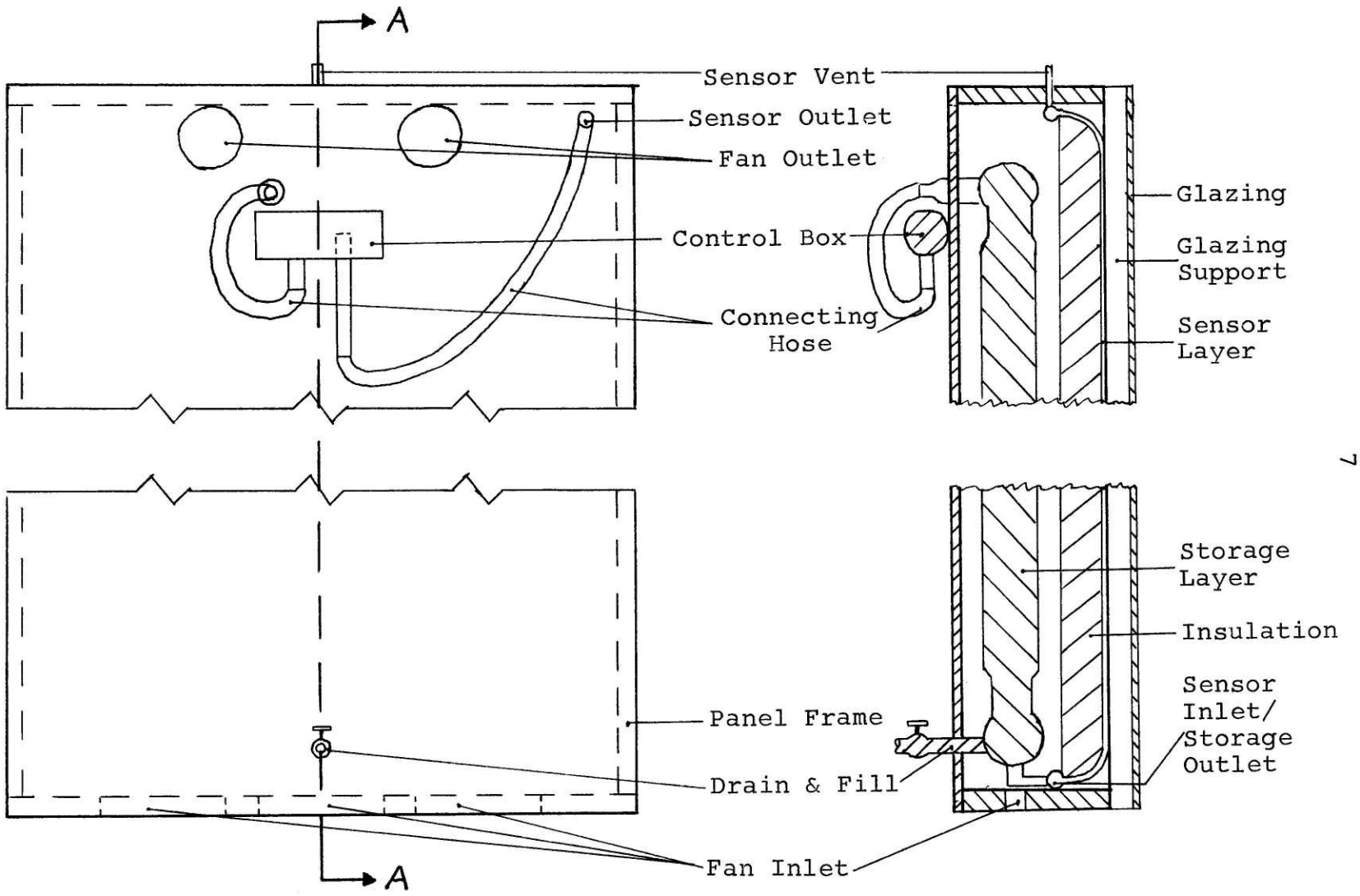

THERMIC PANEL

FIGURE 1

The control box prevents flow of the hot storage water to the cooler sensor layer. An explanation of the control box operation may be found in Appendix A. A more complete description of the panel fabrication appears in Appendix B.

CHAPTER I

TESTING FACILITY AND INSTRUMENTATION

1.1 Test Shed

A test shed was built to test the effectiveness of drawing heat off the storage layer by a forced convection system. The shed is facing South with the panel mounted at a 45 degree angle, as shown in Figure 2. Insulation was placed around the outside edge of the panel to limit any heat loss due to conduction. The panel was also insulated from the inside of the shed to prevent heat flow from the panel to the shed at times when the fans were off.

The shed has been instrumented to monitor solar flux, wind velocity, outside ambient temperature, and average shed temperature. The solar flux meter is a thermopile manufactured by the International Thermal Instrument Company (Model C-155) and generates a DC millivolt signal accurate to 5%. The anemometer was manufactured by Taylor Sybron Corporation (Model #3105). It uses revolving cups to produce an AC signal. The wind velocity is read off a meter supplied with the anemometer.

Temperatures were measured with thermocouples.

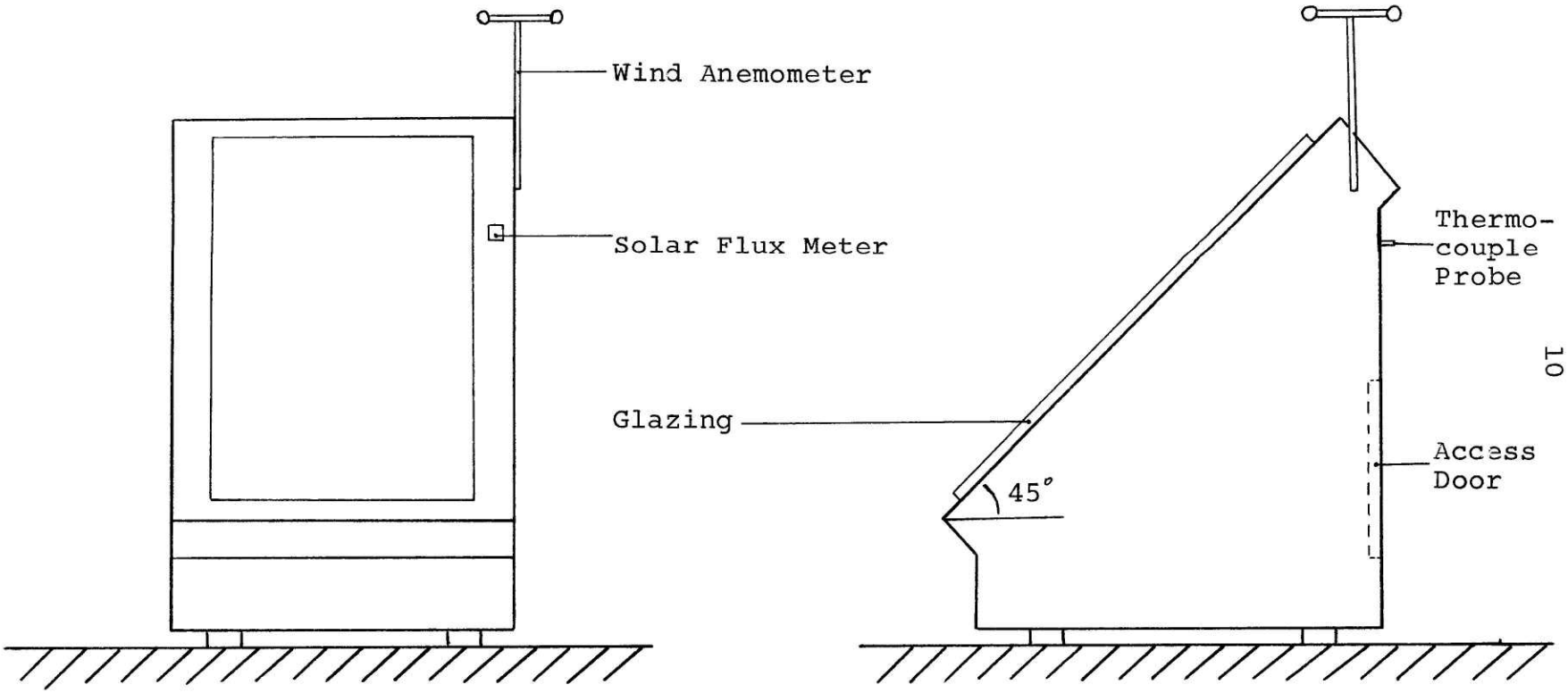

TEST SHED

FIGURE 2

To correct for possible temperature gradients within the shed three thermocouples were used to obtain an average temperature. Outside the shed two thermocouples were used to obtain an average ambient temperature. Details of the instrumentation calibration and installation may be found in Appendix C.

1.2 Solar Panel

Thermocouples were placed at regular intervals along the length of the sensor layer and storage layer. When connected in parallel the average temperature could be monitored. The thermocouples could also be read individually to obtain a temperature profile.

To determine the heat flow between the sensor and storage layers the fluid flow rate and temperature difference between top and bottom of the sensor layer are required. Thermocouples were placed at the connections between sensor and storage layers. The simplest flow measuring method is to use a dye marker in a length of clear Lexan tube. The meter may then be calibrated by measuring the time required for the dye to pass between two reference marks at known mass flow rates. In this panel, the flow meter was integrated into the control box.

1.3 Data Recording

To record the many parameters being monitored a multiplexer was used. The multiplexer mechanically cycles through 10 channels sequentially. The output is then fed to a single pen strip chart recorder. Thus, each channel can be recorded several times each hour.

CHAPTER II

THERMODYNAMICS AND HEAT TRANSFER ANALYSIS

2.1 Heat Transfer to Sensor Layer

Not all of the incident solar radiation is absorbed by the sensor layer. Some is reflected by the glazing. The fraction transmitted to the sensor layer is given by the transmittance (τ) of the glazing. To determine the incident solar radiation absorbed, the sensor layer's absorptance (α) must also be taken into account. The percentage absorbed by the sensor layer is $\tau\alpha$, with $(1-\alpha)\tau$ being reflected as mostly diffuse radiation. Some of this diffuse radiation is reflected back to the sensor layer. The reflections continue until the fraction ultimately absorbed is given by: [1]

$$(\tau\alpha) = \frac{\tau\alpha}{1-(1-\alpha)\rho_d} \qquad (1)$$

where, $(\tau\alpha)$ = Transmittance-absorptance product

ρ_d = Diffuse reflectance

The transmittance of the galzing varies as a function of incidence angle (θ_i) to the glazing. At an incidence angle of $\theta_i = 0$, the maximum solar energy transmission is 77%. Calculations for as a function of may be found in Appendix D. The sensor layer has an

absorptance similar to that of black paint. The absorptance was assumed to be $\alpha = 0.9$. The glazing was modeled as a two glass cover system with a diffuse reflectance of approximately $\rho_d = 0.24$. Thus equation (1) reduces to:[1]

$$(\tau\alpha) = 1.025 * \tau * \alpha \qquad (2)$$

A schematic of the sensor layer heat flows, thermal resistances and representative temperatures are shown in Figure 3. There will be heat transfer losses from the sensor layer caused by conduction, natural and forced convection, and radiation. The only conduction losses present are through the insulation to the storage layer. Calculations prove the conduction loss to be small (Appendix E-1). A numerical analysis of the theoretical convection and radiation heat transfer coefficients is worked out in Appendices E-2 and E-3. From the values an overall heat transfer coefficient (U_{sensor}) can be determined. Thus, the heat loss from the sensor can be given by:

$$QL_1 = U_{sensor} * A * (TT_{avg} - TA) \qquad (3)$$

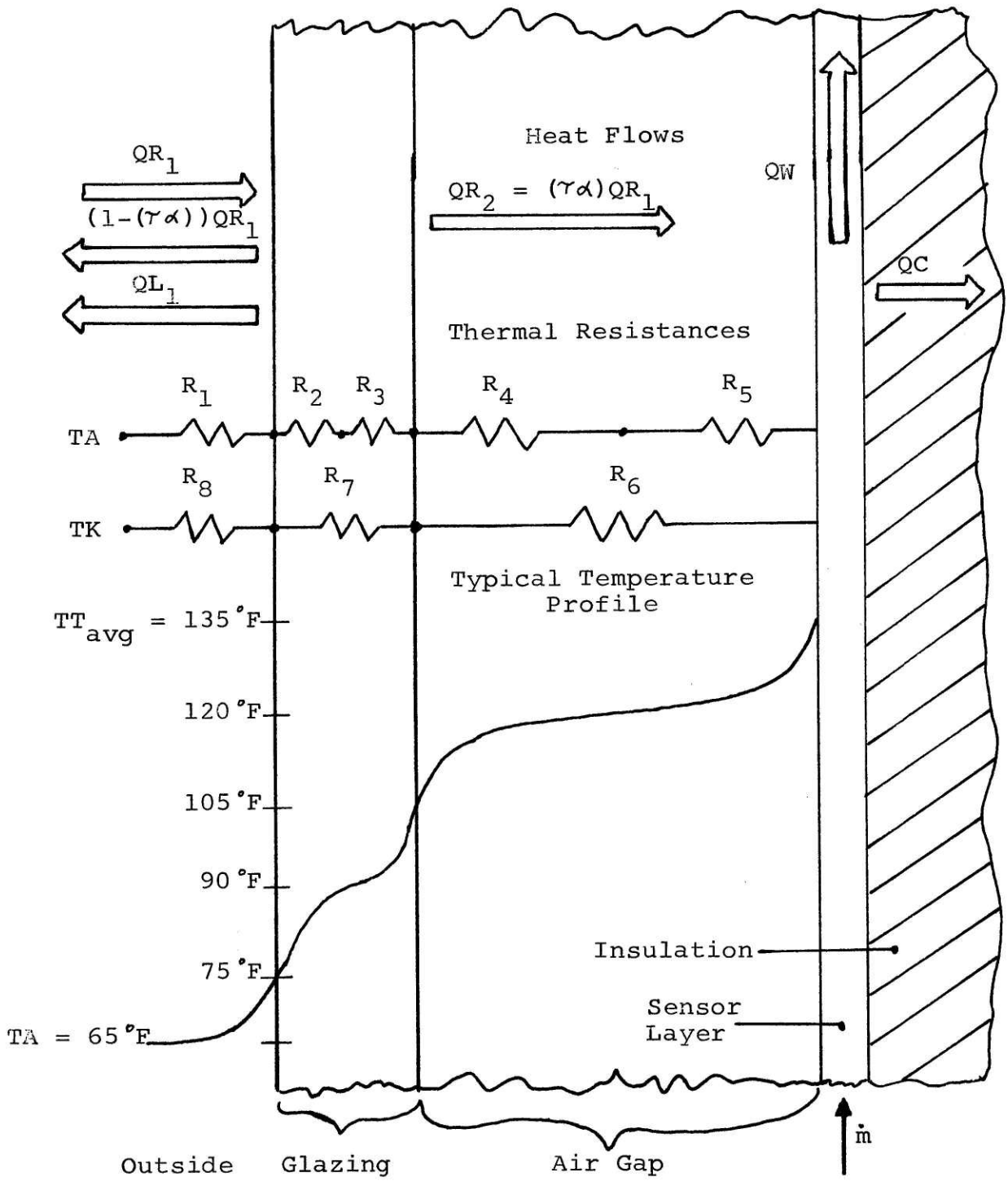

SENSOR LAYER HEAT FLOWS

FIGURE 3

where, QL_1 = Theoretical Heat loss from sensor layer (BTU/hr.)
TT_{avg} = Average sensor layer temperature (°F)
TA = Ambient temperature (°F)
U_{sensor} = Overall sensor heat transfer coefficient ($BTU/hr.ft^2°F$)
A = Area of panel (ft^2)

The overall heat transfer coefficient from equation (3) can be compared with the experimental data. The incident solar radiation can be measured directly. The radiation absorbed by the sensor can be calculated from

$$QR_2 = (\tau\alpha)*QR_1 \qquad (4)$$

where, QR_2 = solar radiation to sensor (BTU/hr)
QR_1 = Incident solar radiation (BTU/hr)

The net heat flow into the sensor layer water can be calculated from the measured parameters:

$$QW = Cp_{water}*\dot{m}*(TT_0 - TT_{10}) \qquad (5)$$

where, QW = Net heat flow into sensor water (BTU/hr)
Cp_{water} = Heat capacity of water (BTU/lbm °F)
$\dot{m}$ = Mass flow rate of water through sensor (lbm/hr)
TT_0 = Sensor layer outlet temperature (°F)
TT_{10} = Sensor layer inlet temperature (°F)

The change in the internal energy of the sensor layer must also be accounted for.

$$\Delta UT = Cp_{water} * m_t * \Delta TT_{avg} \qquad (6)$$

where, ΔUT = Change in internal energy of sensor in past hour (BTU/hr)

mt = Mass of water in sensor layer (= 15.9 lbm)

ΔTT_{avg} = Change in sensor layer average temperature in past hour (°F)

The heat loss from convection and radiation is therefore:

$$QL_2 = QR_2 - QW - \Delta UT \qquad (7)$$

where, QL_2 = Empirically determined heat loss from sensor layer (BTU/hr)

2.2 Heat Transfer to Shed

Once the storage layer has been heated the heating capability of the panel can be measured. One method is to turn on the fans and measure the heat flow into the test shed. This requires knowledge of the shed temperature, outside temperature and an overall heat transfer coefficient for the shed.

The temperature can be easily measured. The heat

transfer coefficient was calculated by measuring the heat heat flow into the shed and taking hourly temperature measurements. The heat capacity and heat transfer coefficient can be determined from:[2]

$$QH_1 = Cp_{shed} \frac{\Delta TH}{\Delta t} + U_{0mph}(TH - TA) \qquad (8)$$

where, QH_1 = Measured heat input to shed (BTU/hr)
Cp_{shed} = Heat capacity of shed (BTU/hr°F)
ΔTH = Change in shed temperature between measurements (°F)
Δt = time interval between measurements (hr)
U_{0mph} = Shed heat transfer coefficient at 0 mph (BTU/hr °F)
TH = Average shed temperature (°F)

The test was done on a cloudy day with no solar radiation and winds about 0 mph. The heat flow was supplied by an electric space heater and measured with a watt-hour meter. The data and calculations for the shed calibration appear in Appendix F-1. The results were Cp= 58.3 BTU/°F and h = 57.7 BTU/hr °F.

The shed heat capacity will remain constant but the shed coefficient, U_{shed}, is a function of wind velocity. To determine the relationship another test was run. This time the shed temperature was maintained approximately

constant with a thermostat on the space heater. The test was run on a day with winds averaging 5 mph. The new heat transfer coefficient is given by

$$QH_1 = U_{5mph}(TH-TA) \quad (9)$$

where, U_{5mph} = Shed heat transfer coefficient at 5 mph (BTU/hr ° F)

The data and calculations for U_{5mph} are in Appendix F-2.

Comparing the shed coefficients U_{0mph} and U_{5mph} and assuming a linear relationship with wind velocity gives:

$$U_{shed} = 57.7 + 1.26\ V \quad (10)$$

where, U_{shed} = Overall heat transfer coefficient (BTU/hr F)
V = Wind velocity (mph)

The shed coefficient and heat capacity given above can be used to determine the heat flow from the storage layer.

$$QS_1 = U_{shed}*(TA - TH) - Cp_{shed} * (\Delta TH) \quad (11)$$

where, QS_1 = Forced convection heat flow from the storage layer(BTU/hr)

The heat flow, QS_1, may be integrated over the time interval when the fans are running to obtain the total heat drawn off the storage section. This should be equivalent with the change in internal energy of the storage layer given by:

$$\Delta US = ms * Cp_{water} * \Delta TS_{avg} \quad (12)$$

where, ΔUS = Change in internal energy of the storage layer (BTU)

ms = Mass of storage layer

ΔTS_{avg} = Change in average storage layer temperature (°F)

Having calculated the heat flows one may now define various efficiencies for the panel.

$$\eta_{collector} = \frac{QW}{QR_1} \quad (13)$$

where, $\eta_{collector}$ = Fraction of incident solar radiation transfered to the storage layer

$$\eta_{sensor} = \frac{QW}{QR_2} \quad (14)$$

where, η_{sensor} = Fraction of solar radiation absorbed by sensor which is utilized

$$\eta_{panel} = \frac{\Delta US_{day}}{\Sigma QR_1} \qquad (15)$$

where, η_{panel} = Fraction of total incident solar radi radiation stored in the panel in one day

ΔUS_{day} = Chang in US during one day (BTU)

ΣQR_1 = Total incident solar radiation for for one day (BTU)

CHAPTER III

TEST RESULTS

3.1 General Trends

One full day test was run. The raw data is tabulated in Table 1. The reduced data giving the heat flows and efficiencies for Chapter III appear in Table 2.

In the morning small amounts of incident sunlight are absorbed by the panel. The sensor layer slowly heats up until at 8:30 am the pressure differential is large enough to initiate flow. As the sun rises, the solar radiation absorbed by the sensor layer rises sharply. This is because the rise of incident solar radiation in the morning is augmeneted by the rise in the transmittance-absorptance product ($\tau\alpha$).

At 8:55 am a maximum mass flow rate is reached. As the day progresses, the mass flow rate steadily declines. The declining mass flow rate is offset by the increasing sensor layer temperature which leads to higher heat flows (QW) from the senor to storage layer. This trend continues until the mid-day when the incident radiation (QR_1) levels out and begins to decline. The heat flow (QW) remains high until 3:30 pm. The incident radiation remains high (about 75%) but the drop in ($\tau\alpha$) to below 50% and the rise in storage layer temperature

Time	8:00 am	8:30	8:55	10:00	10:15	11:00	11:15	12:00
Wind Velocity V (mph)	3	4	3	5	5	-	7	-
Mass Flow Rate (sec)	No Flow	10	6.5	7.2	7.2	-	8.0	-
Direct Solar Radiation (mv)	0.8	1.42	1.75	3.11	3.51	3.2	3.8	3.6
Solar Flux Meter Temp. TQR (°F)	55	60	66	72	75	76	77	82
Average Storage Temp. TS_{avg} (°F)	56	58	57	63	66	73	74	83
Average Sensor Temp. TT_{avg} (°F)	56	72	76	85	87	98	104	123
Sensor Outlet Temp. TT_0 (°F)	52	65	78	102	107	123	129	151
Sensor Inlet Temp. TT_{10}(°F)	52	55	54	54	54	54	58	57
Shed Temperature (°F)	59	60	65	64	68	65	68	68
Ambient Temperature (°F)	53	57	56	58	60	60	60	65

TEST DATA (5-9-76)

TABLE 1

Time	12:20 pm	1:00	1:15	2:10	3:20	3:50	4:05	5:15
Wind Velocity V (mph)	5	-	7	3	2	4	3	4
Mass Flow Rate (sec)	10.5	-	10.5	-	17.0	21.0	35.0	No Flow
Direct Solar Radiation (mv)	4.5	4.3	4.1	4.2	3.4	3.1	2.5	1.9
Solar Flux Meter Temp. TQR (°F)	77	86	80	85	89	85	84	74
Average Storage Temp. TS_{avg} (°F)	87	92	93	98	105	107	106	104
Average Sensor Temp. TT_{avg} (°F)	128	145	147	158	169	169	165	146
Sensor Outlet Temp. TT_0 (°F)	156	171	174	181	192	186	183	151
Sensor Inlet Temp. TT_{10} (°F)	52	53	53	62	79	85	81	89
Shed Temperature (°F)	68	67	69	70	76	78	78	79
Ambient Temperature (°F)	60	65	64	66	73	74	73	72

TEST DATA (5-9-76)

TABLE 1 (cont')

Time	8:30 am	8:55	10:00	11:00	12:00
Mass Flow Rate $\dot{m}$ (lbm/sec)					
Measured	40.0	64.8	57.6	53.9	44.2
Theoretical	13.2	41.5	65.3	52.0	41.9
Direct Radiation QR_1 (BTU/hr ft^2)	93.5	114.1	200.8	204.5	227.8
Transmittance-Absorptance Product ($\tau\alpha$)	.212	.322	.540	.641	.687
Radiation Absorbed by Sensor QR_2					
(BTU/hr ft^2)	29.2	48.5	128.5	151.5	179.3
(BTU/hr)	816.8	1358	3598	4243	5020
Heat to Sensor Water QW (BTU/hr)					
Measured	400	1555	2765	3586	3964
Theoretical	132	996	3137	3589	3940
Heat Loss From Sensor QL_1 (BTU/hr)					
Measured	-	-	690	450	659
Theoretical	176	235	318	447	682
Sensor Efficiency η_{sensor}	49.0%	114.5%	76.8%	84.5%	79.0%
Collecter Efficiency $\eta_{collecter}$	13.9%	44.2%	44.7%	56.9%	56.5%

TABLE 2 REDUCED DATA (5-9-76)

Time	1:00 pm	2:10	3:20	3:50	4:05
Mass Flow Rate $\dot{m}$ (lbm/sec)					
Measured	38.0	31.9	24.6	20.7	14.6
Theoretical	39.8	36.6	15.3	9.2	6.1
Direct Radiation QR_1 (BTU/hr ft^2)	269.3	263.0	210.7	194.1	156.5
Transmittance-Absorptance Product ($\tau\alpha$)	.694	.636	.415	.276	.254
Radiation Absorbed by Sensor QR_2					
(BTU/hr ft^2)	213.8	193.6	108.5	73.0	55.3
(BTU/hr)	5988	5420	3038	2043	1549
Heat to Sensor Water QW (BTU/hr)					
Measured	4472	3800	2780	2091	1489
Theoretical	4697	4131	1734	926	377
Heat Loss from Sensor QL_1 (BTU/hr)					
Measured	1165	1413	83	-	-
Theoretical	941	1082	1129	1117	870
Sensor Efficiency η_{sensor}	74.7%	70.1%	91.5%	102.3%	104.0%
Collecter Efficiency $\eta_{collecter}$	53.9%	46.9%	42.8%	35.0%	30.9%

TABLE 2 (cont') REDUCED DATA (5-9-76)

has reduced the driving head to a low level. Although the heat flow is minimal, the panel continues to operate until 5:15 pm.

The sensor efficiency (η_{sensor}) remains very high for most of the day. This means the glazing is very effective in minimizing heat losses from the sensor to the outside. Over most of the operating day the heat loss is held to under 30% of QR_2.

The collector efficiency ($\eta_{collector}$) ranges from 14% to 57%. During the bulk of the day, the collector efficiency hovers around 50%. It drops off in the early morning and late afternoon, for during these times the glazing reflects a large percentage of the incident radiation.

3.2 Sensor Layer Temperature Profile

A graph of the sensor layer temperature profile is shown in Figure 4. Before flow begins, the sensor layer is heated to a nearly uniform temperature. There is a small temperature gradient due to a density stratification within the sensor. At 8:55 am the flow has just begun this is indicated by the nearly vertical temperature profile.

The increasing incident solar radiation (QR_1) leads to a progressively steeper initial temperature gra-

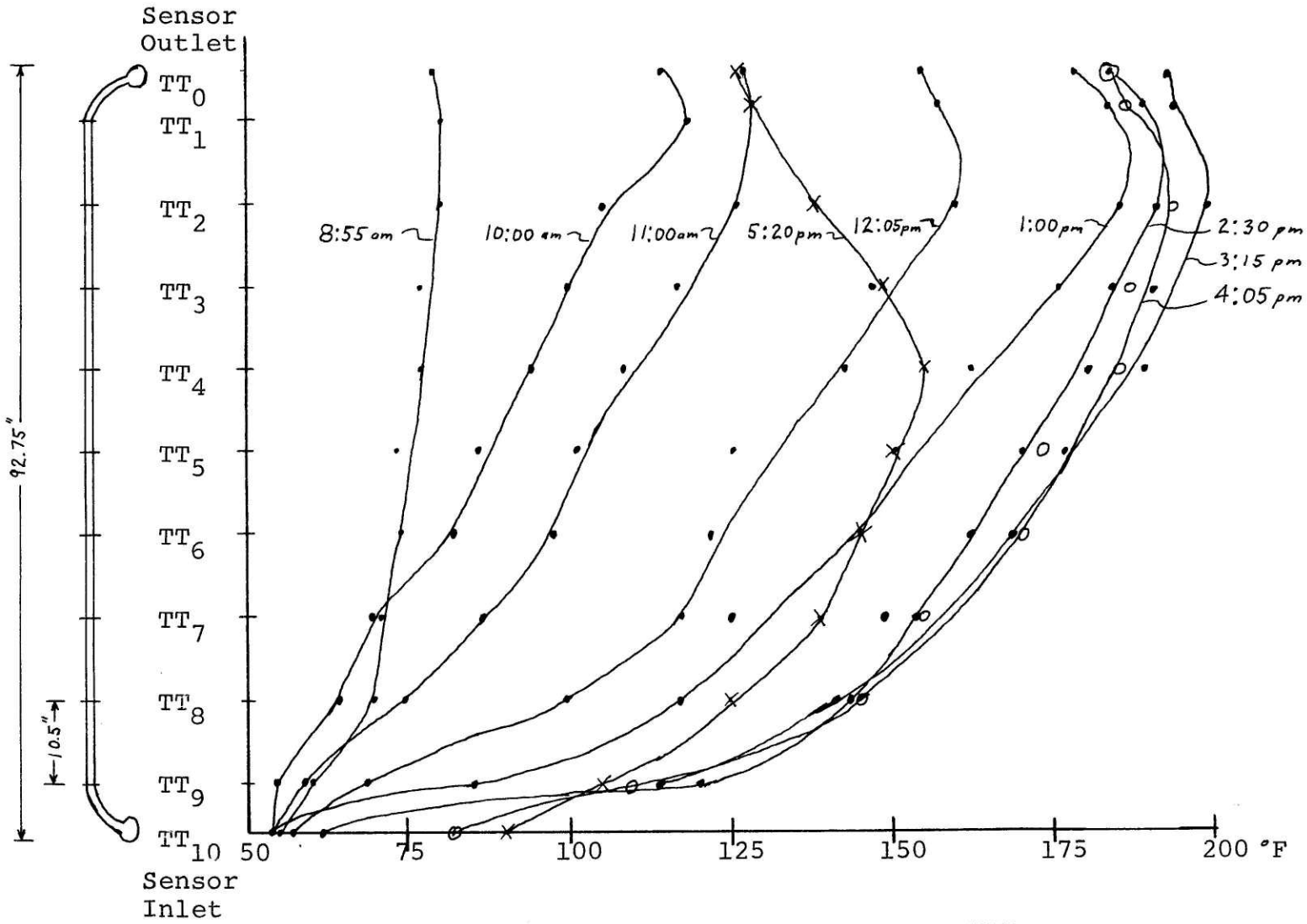

SENSOR LAYER TEMPERATURE PROFILE

(5-9-76)

FIGURE 4

dient. The decreasing mass flow rate also contributes to this trend. When the solar radiation levels out the high initial gradients are maintained, but further up the sensor layer the temperature gradient approaches zero. This is beacause at higher sensor temperatures the heat losses are greater and the temperature approaches an equilibrium. This can be compared with 10:00 am and 11:00 am when the high flow rates lead to a nearly constant temperature gradient.

As the solar radiation declines, the temperature profile does not change much. The initial temperature (TT_{10}) increases due to increasing storage layer temperature. This reduces the heat input neccessary to maintain the high sensor outlet temperature(TT_0). The outlet temperature (TT_0) continues to rise until 3:15 pm. This is because the mass flow continues to decline thus allowing an increment of water to absorb more total solar radiation. At 4:00 pm the longer time of exposure does not compensate for the declining radiation and the sensor temperatures drop.

A sensor profile was not taken at 5:15 pm. However, Table 2 shows the mass flow to be minimal and the average sensor temperature (TT_{avg}) to have dropped 19°F in the last hour. This indicates that the heat loss

caused by the high sensor temperature was much higher than the solar radiation.

3.3 Storage Layer Temperature Profile

A graph of the storage layer profile is shown in Figure 5. Before flow is initiated tha profile shows a small temperature gradient as in the sensor layer. When flow begins the profile indicates the mass and heat flow to be comparable to slug flow.

Between 9:15 and 10:15 am the heated water has moved from TS_1 to TS_3. In the next hour the heated water has moved another thermocouple interval(10 5/8"). This This slug type flow with minimal conduction through the water continues until 12:15 pm. After this time, the peak storage temperature does not rise appreciably. The lower half of the storage layer temperature continues to rise but this is far less than that expected by the measured heat flows (QW).

Unless the water stops moving, there is no reason for TS_1 through TS_9 not to increase with time. To help clarify the discrepancy, horizontal temperature profiles were taken across the storage layer at the approximate position of TS_5. The resulting graph is shown in Figure 6.

The implication is that most of the hot water is

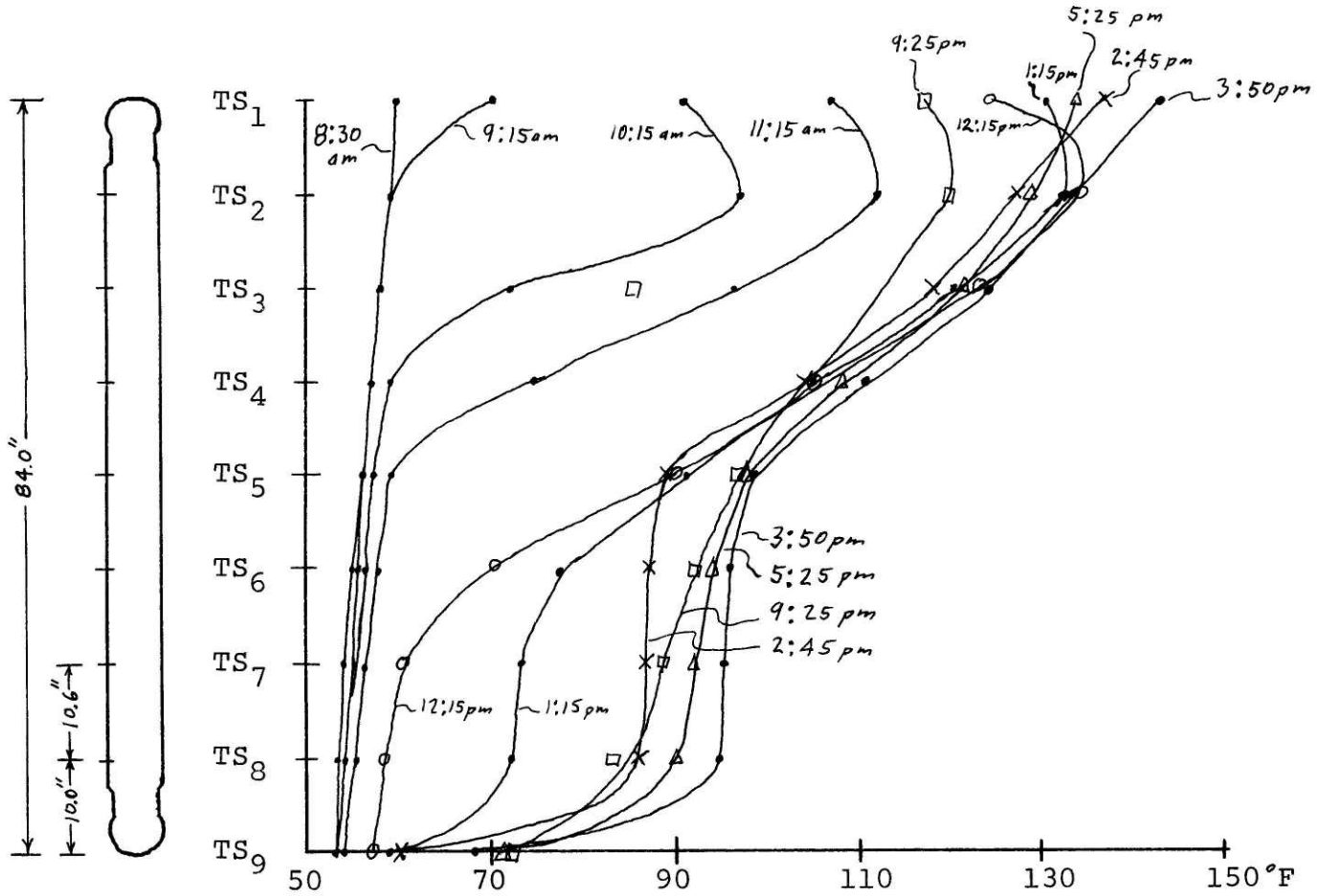

STORAGE LAYER TEMPERATURE PROFILE

(5-9-76)

FIGURE 5

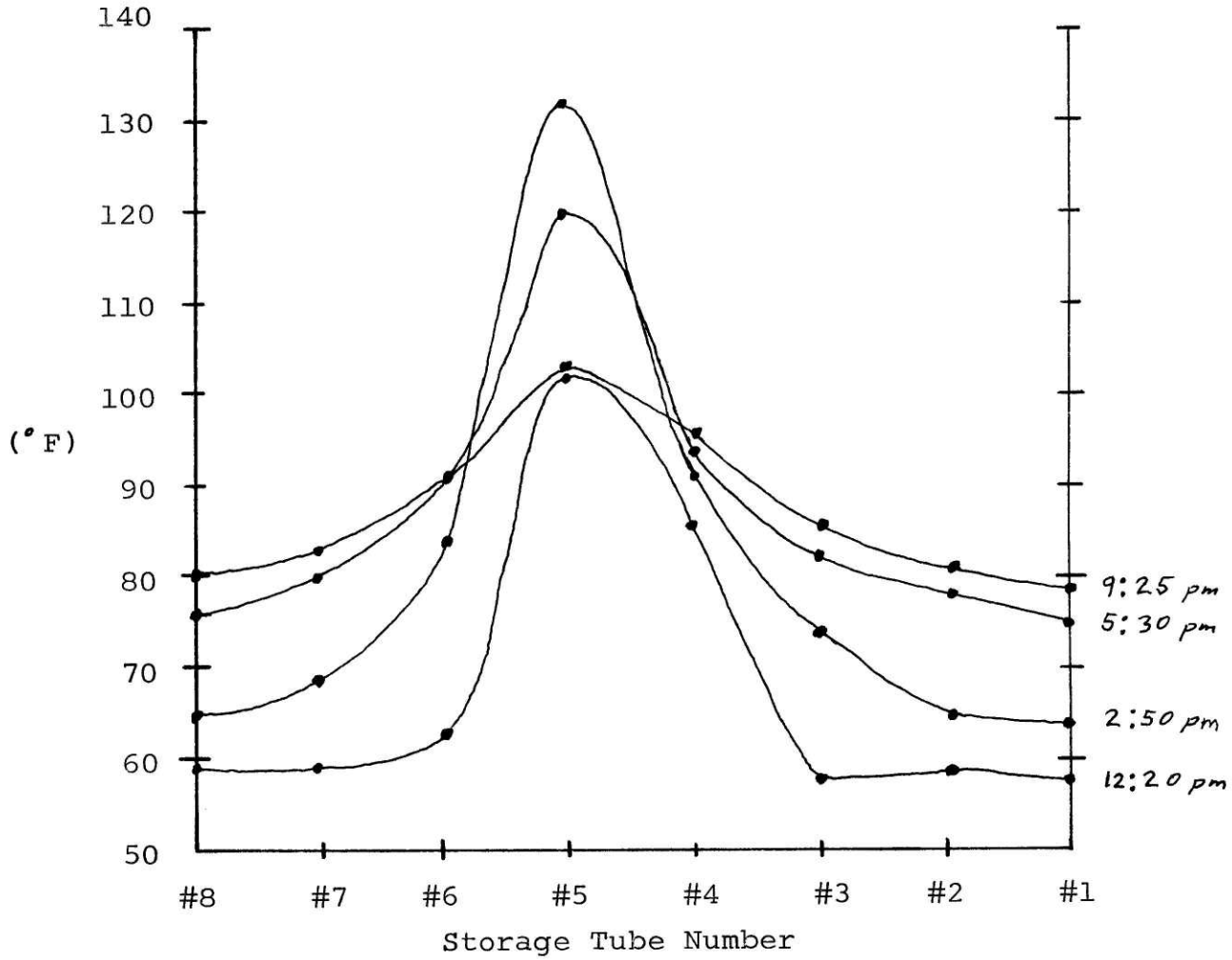

Note:

All thermocouples placed at same height as TS_5.
Storage inlet in top header located between tubes #4 and #5.
Storage outlet in bottom header located between tubes #7 and #8.
Thermocouples for vertical temperature profile were placed along tube #4.

STORAGE LAYER HORIZONTAL TEMPERATURE PROFILE (5-9-76)

FIGURE 6

flowing down storage tubes Numbers 4 and 5. Later in the day a pressure head develops between the cool and hot storage tubes which is sufficient to prevent any mass flow down the hotter tubes. Thus in the afternoon the hotter water from the sensor would be flowing to the outer tubes Numbers 1, 2, 3, 6, 7 and 8. At the end of the day in the absence of flow the pressure head between the storage tubes should eventually drive them to equlibrium. The data shown in Figure 6 tends to support this hypothesis, although more information is required before any conclusion may be drawn.

This also implies that the average storage temperatures measured along tube Number 4 are actually too high. Without a more complete picture of the temperature distribution in the other tubes, it remains unclear how representative the measured temperature profile is of the whole storage layer.

3.4 Heat Storage

By the end of the test day (5:15 pm) the average storage layer temperature had risen 48°F. For the reasons cited in section 3.3, the average storage temperature has dropped to 99°F by 9:25 pm. The true average is not known but we shall assume it to be 99°F.

The change in internal storage layer energy (ΔUS)

during the day is given by Equation (12). The panel efficiency from Equation (15) was calculated to be η_{panel} = 22%. QS should be equivalent to the integral of QW during the day. From the data in Table 1, QS = 12,556 BTU and $\int_{8:30\ am}^{5:15\ pm}$ QW = 25,866 BTU.

Part of the difference can be explained by heat loss between the sensor outlet and storage inlet. Most of the connecting tubing was insulated. The control box and flowmeter were not. The heat loss from the control box is given by:

$$QC = U_{cb} * A_{cb} * (TT_0 - TH) \qquad (16)$$

where, QC = Heat loss from control box (BTU/hr)
U_{cb} = overall heat transfer coefficient of control box 1 BTU/hr ft^2 °F
A_{cb} = Area of control box 1 ft^2

for the assumed values above and an average temperature differnce over the entire day of 78°F, the total heat loss is 680 BTU. This amounts for only 5% of the loss. The discrepancy of this heat loss cannot be explained without further testing.

At night the fans were turned on to heat the shed. Using Equation (11), the heat flow from the storage layer can be calculated. Table 3 gives the measured tempera-

tures and resulting heat flows during the night. The maximum heat flow from the storage layer is 1193 BTU/hr. Integrating the heat flows over the entire night yields a total heat output of 2913 BTU from the storage layer. Since the storage layer temperature in the morning was 56 F the measured fan output was only 23% of the change of internal storage layer energy (ΔUS)

This discrepancy may be explained in part by the circulation system in the shed. With the fans on, the heat transfer coefficient for the inside of the shed will rise because of forced convection. This will increase U_{shed} and the calculated values of QS_1. There will also be conduction losses from storage to the outside but they will be small. Even with these considerations the bulk of the heat loss cannot be accounted for from the data taken.

3.5 Cover System Vented

There was some concern that the glazing might cause the sensor to overheat. The possibility of damaging the sensor is small but boiling the water in the sensor could result in vapor lock. The steam could collect in the top header restricting the flow to the storage section, raising sensor temperatures, and ultimately blocking flow completely.

Time	TH °F	TA °F	(TH - TA) °F	QS_1 BTU/hr
9:10 pm	77	65	12	
Fans turned on at 9:35				-
9:35	79	63	16	
				1192
10:20	78	61	17	
				1142
11:10	77	59	18	
11:25	74	58	16	
QS_1 calculated for time interval (11:10 - 12:10)				515
12:10 am	70	46	14	
Noise in the instrumentation equipment probably caused this inconsistancy in TA. Assume TA = 56				430
1:10	65	54	11	
				460
2:10	63	54	9	
				0
3:10	52	51	1	

Note:
Wind velocity during this time was ~ 0 mph.

NIGHT TEST
(5-9/10-76)

TABLE 3

The sensor temperature could be controlled by venting the cover systems at the top and bottom. The vent runs for the width of the panel between the glazing and sensor layer. With the vents open, there is air flow through the cover system to the outside. This decreases the thermal resistance and adds another heat loss to the system.

Tables 4&5 list the measured parameters, heat flows and efficiencies at several times in the morning and afternoon. In the morning the peak and average sensor layer temperatures are less for comparable amounts of solar radiation. The sensor efficiency drops by about 20%, but the collector efficiency does not change much. This is because the changes in heat loss are a small fraction of the incident solar radiation.

The panel was shut off ($\dot{m}=0$) between 11:30 am and 1:30 pm for other testing purposes. Thus the afternoon results cannot be compared with those of Tables 1 and 2.

3.6 Comparison With Theory

The thermic panel relies on temperature differences between the sensor and storage layers to drive the flow. A greater temperature difference causes a greater density difference. Hence the driving force and flow rate should increase. The data in Table 1 indicates an increasing temperature difference with time and a decreasing

Time	10:20 am	11:00	2:15 pm	3:15	4:10	5:50
Wind Velocity V (mph)	7	5	5	6	5	0
Mass Flow Rate (sec)	6.5	7.0	11.0	10.5	48.5	No Flow
Direct Solar Radiation (mv)	3.44	3.55	3.45	3.98	2.88	1.1
Solar Flux Meter Temp. TQR (°F)	69	73	74	78	76	63
Average Storage Temp. TS_{avg} (°F)	70	75	79	89	91	84
Average Sensor Temp. TT_{avg} (°F)	87	93	104	113	111	83
Sensor Outlet Temp. TT_0 (°F)	100	110	133	129	125	99
Sensor Inlet Temp. TT_{10} (°F)	59	61	71	69	67	73
Shed Temperature (°F)	63	70	66	69	67	73
Ambient Temperature (°F)	56	60	62	64	65	63

TEST DATA (5-8-76)

TABLE 4

Time	10:20 am	11:00	2:15 pm	3:15	4:10
Mass Flow Rate $\dot{m}$ (lbm/sec)	64.6	59.6	36.4	37.4	12.4
Direct Radiation QR_1 (BTU/hr ft^2)	222.1	229.2	220.5	251.8	184.1
Transmittance-Absorptance Product	.586	.641	.613	.443	.235
Radiation Absorbed by Sensor QR_2					
(BTU/hr ft^2)	152.4	169.8	157.2	136.7	61.7
(BTU/hr)	4266	4756	4402	3828	1726
Heat to Sensor Water QW (BTU/hr)	2649	2920	2257	2244	558
Heat Loss From Sensor QL_1 (BTU/hr)	1617-ΔUT	1741	2145 - ΔUT	1441	1200
Sensor Efficiency η_{sensor}	62.1%	61.4%	51.3%	58.6%	32.3%
Collecter Efficiency $\eta_{collecter}$	42.6%	45.5%	36.6%	31.8%	10.8%

REDUCED DATA (5-8-76)

TABLE 5

flow rate. Comparing the begining and the end of the day shows that a temperature difference of 14°F was required to initiate flow, however, the flow stopped with a temperature difference of 42°F. These discrepancies cannot be explained without more test data.

An overall heat transfer coefficient(U_{sensor}) for the sensor layer was calculated in Appendix E-3. For the data listed in Table 1 the theoretical heat loss (QL_1) can be determined from Equation (3). The tabulated comparison between the theoretical and actual results appear in Table 2. Between the hours of 10:00 am and 2:00 pm the results compare favorably. Beyond these bounds, the data would indicate no heat loss. This cannot be true, so I will examine in detail the reasons for the inconsistancy.

At 8:30 am, heat flow has just begun. The sun has been out for a couple of hours. The total heat input from the sun since dawn is what raised the sensor layer temperature. Omitting the ΔUT term, QL_2 = 417 BTU/hr. This is higher than expected but there are many transient effects at the start of flow which could cause this.

At 8:55 am the heat flow into storage is more than the solar heat input. To initiate flow through the control box an initial pressure head is required to over-

come the surface tension effects of oil in the control box. Once flow is established, the pressure drop through the control box decreases and the driving force increases. Thus the mass flow and heat flow into the storage layer are higher than expected.

As the incident solar radiation decreases, so does the heat flow into the storage layer. The discrepancy arises because the change in heat flow (QW) cannot respond as fast as the changing solar radiation. Thus my calculations would indicate a negative heat loss.

There was some question as to the accuracy of the flowmeter. The calibration was done with fully developed flow. When installed in the control box there were problems with boundary layer separation at the entrance to the flowmeter. From the measured temperatures and calculated heat flows the theoretical mass flow rate was also calculated (Equation 5). The results can be found in Table 2. Considering the innacuracies of the system and equations, the results compare favorably. Again, there are large discrepancies in the morning and afternoon when the solar radiation to the panel (QR_2) is changing rapidly.

3.7 Conclusions

Of the total incident solar radiation during one day the sensor layer absorbs 55%, transfers 44% to the storage section, and 22% is saved in the storage layer. The heat losses from the sensor layer to the atmosphere are 11% of the incident radiation and 20% of the radiation absorbed by the sensor. These collector efficiencies are comparable with that of other solar energy systems.

Once the heated water leaves the sensor there are large heat losses to the surrounding air. There are apparently 50% heat losses between the sensor and storage layers. Once the heat is in the storage section there are further losses as the forced air system transfers heat to the shed. Both these losses are unaccountably high, and reduce the percentage of useful energy absorbed by the panel to only 5%.

CHAPTER IV

RECCOMENDATIONS FOR FUTURE WORK

The first step toward obtaining more accurate results is to improve the instrumentaion. The multiplexer is currently set up to sample each channel once an hour. To obtain a clearer indication of trends, the sample rate could be increased.

Thermocouples should be placed in the flow stream whenever possible. Thermocouple wells could easily be installed through most of the panel. Between the sensor outlet and storage inlet there appears to be a large heat loss. This can be documented if thermocouples are used to measure the temperature between these points.

The flowmeter could be improved in several ways. Screens could be used to distribute the flow evenly, a flow straightening section to reduce turbulence, and a convegent section to reduce boundary layer separation. A length of tube should also be provided so the flow may fully develop. To eliminate the human error in the flow measuring scheme, an electric flow measuring device should be used. One possibility is a hot film anemometer.

The wind velocity should also be monitored with an electric signal. An averaging circuit could then be used to obtain a more accurate reading of the average wind velocity.

The large errors in the calculations for QS_1 lead me to believe the shed heat transfer coefficient (U_{shed}) to be unreliable. To recalibrate the shed, a better thermostat should be used to maintain a constant shed temperature. The calibration should also be made with the forced air fans running.

To maintain a uniform horizontal storage temperature profile there should be channels for flow between the tubes of the storage layer. To get a better picture of the flow through the storage layer, thermocouples could be placed on all storage tubes.

The reason for decreasing flow rate with increasing temperature difference (Section 3.6) cannot be explained by the data presented here. After the improvements of the instrumentation mentioned above have been made, a series of tests under controlled conditions can be run.

One of the difficulties of trying to analyze this discrepancy are the dramatic changes in incident solar radiation. The first test would be to determine the mass flow rates, equilibrium temperatures and temperature profiles for a constant uniform heat input. In steady state the driving pressure could be calculated, the mass flow accurately measured, and an empirical relationship between them determined. Then studies could be made of the mass flow rate with a time varying heat input.

APPENDIX A

CONTROL BOX OPERATION

The control box is shown in Figure 7. The function of the control box is to allow heat and mass flow in one direction with small driving pressures, and to prevent flow in the opposite direction.

As the sensor layer heats up in the morning its density decreases. The cooler storage layer water with higher density will eventually push the oil-water interface over the top of the sensor tube. To initiate flow with the minimum possible pressure differential it is desirable to have the top of the tube just above the oil-water interface.

As the sun sets the driving pressure is reversed. The cooler sensor layer pushes the storage water against the oil-water interface. This drives the oil down the sensor tube until the pressure head from the temperature difference is balanced by the oil-water density difference. With no mass flow through the control box the only heat flows are conduction losses through the panel insulation and through the water to the outside.

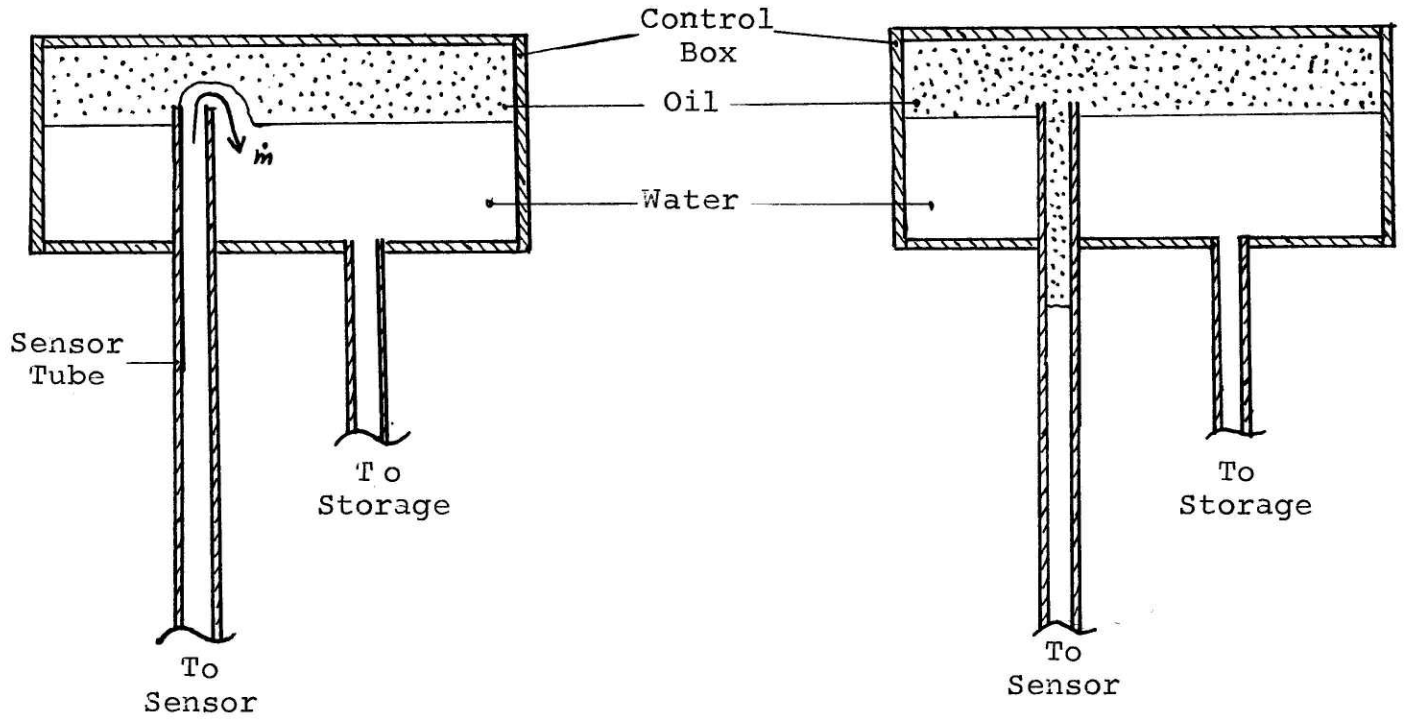

Figure 7A - Daytime Operation

Figure 7B - Nighttime Operation

CONTROL BOX OPERATION

FIGURE 7

APPENDIX B

PANEL FABRICATION

The panel sensor layer dimensions are approximately four foot by eight foot by one-eighth inch thick. The total area exposed to the sun is 28 ft^2. It was fashioned from a FAFCO solar collector.

The collector is an extruded polypropylene sheet containing about 200 rectangular channels (1/8"x3/16") over its four foot width. The headers at each end were made from two inch diameter polypropylene tubes. A plastic welder was used to fit them to the FAFCO collector. The headers were bent back into the panel to limit the possibility of freezing and bursting the headers.

The storage layer was made with four inch diameter thin wall PVC drain pipe. It was assembled using commercially available fittings. Connections between the sensor layer, storage layer and control box were made with one inch diameter Vincon tubing, radiator hose, and hose clamps.

The top of the sensor layer was vented to an overflow tank. This was to prevent any air in the system from becoming trapped in the header and restricting flow. It is also used to absorb the volume changes of the panel as the storage layer is heated. The volume of water was observed to change by as much as .067 ft^3 or 1.4%.

The cover system was a Sun-Lite Glazing panel purchased

from the Kalwall Corporation. It is made of two Sun-Lite Premium fiberglass sheets 0.040" thick bonded to extruded aluminum I-beams to space then one-half inch apart. The glazing was mounted on the solar panel with a one and one-half inch spacing.

The insulation used in the panel was a closed cell foamed plastic. The frame for the panel was of wood with a plywood backing.

APPENDIX C

INSTRUMENTATION

APPENDIX C-1 Solar Flux Meter

The solar flux meter is temperature sensitive, such that the output signal is a function of its operating temperature. Therefore it was mounted on an aluminum plate with a high heat capacity to maintain a relatively constant operating temperature. The meter temperature was monitored so the output could be corrected for temperature. To minimize wind effects the meter was covered with a watch glass.

The watch glass has a transmissivity of about $\tau_{glass} = 0.9$.[3] To correct for this loss the meter output was multiplied by a factor of 1/0.9 or 1.11. The meter is a pyrheliometer which measures only direct solar radiation. The total incident radiation is the sum of the direct and diffuse radiation. Examination of direct and diffuse radiation measurements indicates that the contribution from the diffuse radiation is approximately 10% of the direct radiation. Thus the measured radiation was multiplied by a factor of 1.10 to obtain a more realistic value for the total incident radiation.

APPENDIX C-2 Wind Anemometer

To aid in recording wind speed a circuit was built to rectify the AC output, filter out all high frequency fluctuations (gusts of wind) and give a DC output proportional to

average wind speed.

The circuit worked but did not respond to winds below ten mph. The circuit is being revised and was not used for these tests. The hourly wind measurements listed in the data were sampled over a short time interval and are not as accurate as the proposed averaging circuit.

APPENDIX C-3 Thermocouples

The ambient temperature thermocouples were mounted on the North side of the shed to keep them in the shade. They were encased in capped Lexan tubes to reduce wind influences and to dampen any transient effects. The ambient temperature thermocouples were covered with reflective foil to eliminate errors from diffuse radiation. Thermocouples in the shed were installed the same way but without the reflective foil.

The thermocouples for the sensor and storage layers were not installed in the flow but mounted on the outside surface. The conductivity for both PVC and polypropylene is about 0.11 BTU/hr ft °F.[4] The wall thicknesses for the sensor and storage layers are 0.018" and 0.063" respectively. The heat transfer coefficient on the other side of the thermocouple is assumed to be 1.0 BTU/hr ft^2 °F. For these numbers the temperature measurement errors should be 1.4% for the sensor and 2.3% for the storage layer.

These calculations assume a good thermal contact between the thermocouple and the wall. The thermocouples were first

soldered to 0.5" square copper foil for easier handling. They were then taped to the appropriate surface. The presence of any air gap would lead to errors in the temperature reading. The thermocouples should have been bonded to the walls with a high thermal conductivity epoxy.

APPENDIX D

GLAZING TRANSMISSIVITY

The transmissivity of the Sun-Lite glazing is a strong function of incidence angle. The following information was supplied with the glazing:

TABLE 6

SOLAR ENERGY TRANSMISSION

Transmissivity (τ)	Incidence Angle (θ_i)
77%	0
73%	30
65%	45
48%	60

Thus the incidence angle as a function of time is required to determine τ, $(\tau\alpha)$ and hence QR_1 during the day. A plot of altitude (θ_{alt}) vs. azimuth (θ_{az}) was obtained for this time of year in the Boston area (Figure 8). For a panel facing South at a 45° angle with the horizen, the incidence angle (θ_i) is given by:

$$\cos(\theta_i) = \cos(\theta_{az})*\cos(\theta_{alt}-45) \qquad (17)$$

Values for the transmittance can be interpolated from Table 6 and a plot of transmittance (τ) as a function of time drawn (See Figure 8).

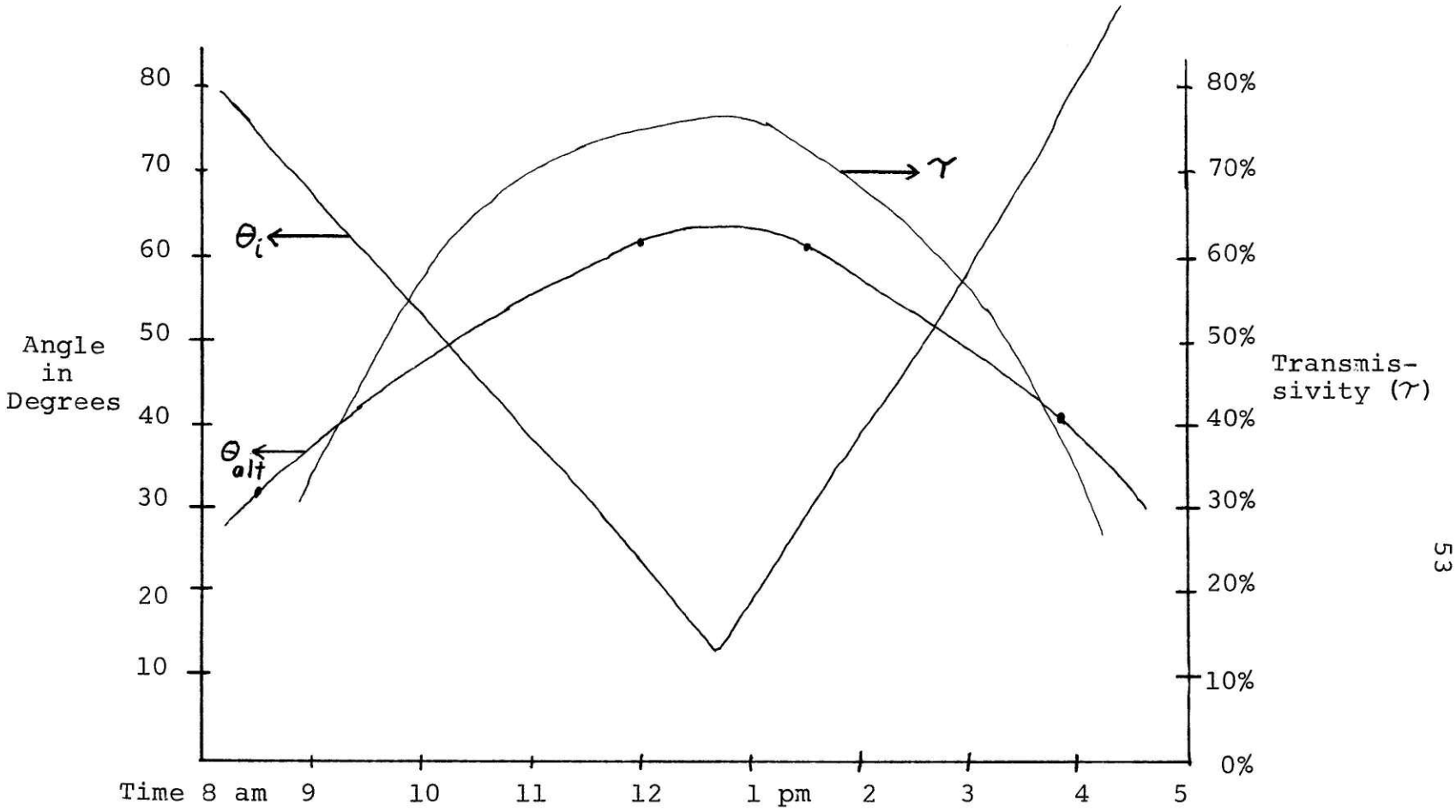

θ_{alt} vs. time plot reproduced with the permission of D.K.Hoshizaki.

θ_{alt}, θ_i, and τ vs. time

FIGURE 8

APPENDIX E

SENSOR LAYER HEAT LOSSES

APPENDIX E-1 Conduction Losses

The conductivity (k_{foam}) for the closed cell foamed plastic insulation was assumed to be equivalent to that of polystyrene k_{foam}=0.021 BTU/hr ft °F.[4] The insulation thickness (x_{foam}) is three inches. The maximum difference between the average sensor and storage layer temperatures was 64 F. The conduction heat loss is given by:

$$QC = (k_{foam}/x_{foam}) * A * (TT_{avg} - TS_{avg}) \quad (18)$$

where, QC = Conduction loss (BTU/hr)

A = Area of insulation (°F)

For the values listed above, the maximum heat loss would be 172 BTU/hr. This is less than 3% of the incident solar radiation absorbed. The average value during the day is about 2%.

APPENDIX E-2 Convection Losses

The air gaps in the cover system are large enough for there to be natural convection. If the sensor layer and glazing are modeled as vertical plates, the natural convection heat transfer coefficient (h_{nc}) is:[2]

$$h_{nc} = 0.21 * (\Delta T)^{1/3} \quad (19)$$

where, ΔT = Temperature difference across surface-air interface (°F)

For normal operating conditions ΔT will be approximately

$(TT_{avg} - TA)/4 \approx 15°F$ across all interfaces. The thermal resistances are (refer to Figure 3):

$$R_2 = R_3 = R_4 = R_5 = \frac{1}{h_{nc} * A} = \frac{1.93}{A} \frac{hr\ ft^2\ °F}{BTU}$$

The thermal resistance R_1 varies with wind velocity from a maximum resistance equal to that for natural convection to a minimum value near zero in high winds.

APPENDIX E-3 Radiation Losses

The radiation heat flow between two parallel plates is:[2]

$$QR_{1-2} = A * F_{12} * \sigma * (T_1^4 - T_2^4) \qquad (20)$$

where, QR_{1-2} = Radiation from surface 1 to surface 2 (BTU/hr)
A = Area of surface 1 (ft^2)
F_{12} = View factor 0.9
σ = Stefan-Boltzman constant = $0.1713 * 10^{-8}$ BTU/hr ft^2 $°R^4$
T_1 = Temperature of surface 1 (°F)
T_2 = Temperature of surface 2 (°F)

For small temperature drops Equation (20) can be linearized.[5]

$$QR_{1-2} \approx 4 * F_{12} * \sigma * (T_{avg})^3 * (T_1 - T_2) \qquad (21)$$

where, $T_{avg} = (T_1 + T_2)/2$

Assuming an average temperature of 120°F in the air gap, 90 °F in the glazing, 65°F outside, and a sky temperature of:[1]

$$TK = TA - 11 \qquad (22)$$

where, TK = Sky temperature during the day (°F)

The thermal resistances calculated from Equation (21) are $R_6 = 1.20$, $R_7 = 1.03$, and $R_8 = 0.92$ BTU/hr ft^2 °F.

APPENDIX E-4 Overall Sensor Heat Transfer Coefficient

The overall heat transfer coefficient (U_{sensor}) can be calculated by combining the thermal resistances. With no wind, U_{sensor} = 0.43 BTU/hr ft^2 °F. With strong winds U_{sensor}= 0.58. The exact relationship between U_{sensor} and wind velocity is not known. Therefore an average value will be used. All data in Tables 2 & 3 assumes a value of U_{sensor} = 0.49.

APPENDIX F

SHED CALIBRATION

APPENDIX F-1 Wind = 0 MPH

The data from this test is shown in Table 7. The space heater was always running, thus the heat input to the shed was constant, QH_1 = 3891 BTU/hr. The first time interval (2:00 pm-2:30 pm) was not used in the reduced data to allow for initial transients and the opening of the shed door (an unmeasurable heat loss). The same is true of the last test reading when the shed door was again opened. For the time intervals listed below, the data gives an empirically determined relationship between heat input (QH_1), shed heat capacity ($C_{p\ shed}$), and heat transfer coefficient for the shed ($U_{0\ mph}$). See Equation(8).

TABLE 8

SHED CALIBRATION - REDUCED DATA

Time Interval	Heat Flow
2:30 - 3:30 pm	3891 BTU/hr = $C_{p\ shed}$ * (19.2) + $U_{0\ mph}$ * (49.5)
3:17 - 4:17 pm	3891 BTU/hr = $C_{p\ shed}$ * (9.0) + $U_{0\ mph}$ * (60.0)
4:17 - 5:17 pm	3891 BTU/hr = $C_{p\ shed}$ * (3.0) + $U_{0\ mph}$ * (66.0)

From the expressions in Table 6 the relationship between $C_{p\ shed}$ and $U_{0\ mph}$ is:

$$C_{p\ shed} = 1.01 * U_{0\ mph} \qquad (23)$$

Time	2:00 pm	2:30	3:17	4:17	5:17	5:30	7:45
Shed Temperature TH (°F)	96	102	117	126	129	129	111
Ambient Temperature TA (°F)	58	60	60	63	60	61	59
(TH - TA) (°F)	38	42	57	63	69	68	52
Watt-hour Meter Reading (kw-hr)	10.0	-	-	-	-	-	16.5
Heat Input to Shed (BTU/hr)	3891	3891	3891	3891	3891	3891	3891

Note:
Average wind velocity during this time was ~ 0 mph

SHED CALIBRATION (5-7-76)

TABLE 7

Using Equation (23) in Table 6 gives $U_{0\ mph}$ = 57.7 BTU/hr °F and $C_{p\ shed}$ = 58.3 BTU/°F.

APPENDIX F-2 Wind = 5 MPH

Table 9 lists the data when a constant shed temperature (TH) was presumably maintained. The fluctuations in TH indicate the thermostat controlling the heater had a slow response time.

From the data an average shed temperature was assumed TH = 99.4 F. For the $C_{p\ shed}$ calculated in Appendix F-1, the heat required to bring the shed up to the average temperature from its initial temperature is:

$$C_{p\ shed} * (99.4 - 90.0) = 548 \text{ BTU} \qquad (24)$$

For a total heat input to the shed of 29693 BTU, the average hourly heat flow is:

$$(29693 - 548) \text{ BTU}/11.3 \text{ hr} = 2579 \text{ BTU/hr} \qquad (25)$$

Equation (9) gives $U_{5\ mph}$ = 64.0 BTU/hr ft^2 °F. Assuming a linear relationship between U_{shed} and wind velocity:

$$U_{shed} = 57.7 + 1.26\ V \qquad (10)$$

Time	9:40 pm	2:20 am	3:20	4:20	5:20	6:20	9:00
Shed Temperature TH (°F)	90	102.5	100	95	95	94	105
Ambient Temperature TA (°F)	68	63	58	54	52	53	69
(TH - TA) (°F)	22	39.5	42	41	43	41	36
Watt-hour Meter Reading (kw-hr)	17.5	-	-	-	-	-	26.2

Note:
Average wind velociy over this time was ~5 mph.

SHED CALIBRATION (5-10/11-76)

TABLE 9

LIST OF APPENDICES

REFERENCES

(1) Duffie,J.A., and W.A. Beckman, Solar Energy Thermal Processes, 1974, John Wiley and Sons.

(2) Rohsenhow,W.M., and H.Y. Choi, Heat,Mass, and Momentum Transfer, 1961, Prentice Hall.

(3) Baumeister, ed., Standard Handbook for Mechanical Engineers, 1967, McGraw Hill Book Co., 7th ed.

(4) Bolz,R., and G. Tuve, ed., Handbook of Tables for Applied Engineering Science, 2nd ed, 1973, The Chemical Rubber Company.

(5) Verbal quote from W.M. Rohsenhow, Course 2.601J, May 1976.